

**CWEX: Crop/Wind-energy EXperiment:
Observations of surface-layer, boundary-layer
and mesoscale interactions with a wind farm**

***Article In Press to:
Bulletin of the American Meteorological Society***

Daniel A. Rajewski^{1*}

Eugene S. Takle², Julie K. Lundquist^{3,4}, Steven Oncley⁵, John H.
Prueger⁶, Thomas W. Horst⁵, Michael E. Rhodes⁷, Richard Pfeiffer⁶, Jerry
L. Hatfield⁶, Kristopher K. Spoth², Russell K. Doorenbos²

¹ Department of Geological and Atmospheric Sciences, Iowa State University, Ames, IA, 50011.

² Department of Agronomy, Iowa State University, Ames, IA, 50011.

³ Department of Atmospheric and Oceanic Sciences, University of Colorado, Boulder, CO, 80309.

⁴ National Renewable Energy Laboratory, Golden, CO, 80401.

⁵ National Center for Atmospheric Research, Boulder, CO 80303.

⁶ National Laboratory for Agriculture and the Environment, Ames, IA 50011.

⁷ Aerospace Engineering Sciences, University of Colorado, Boulder, CO, 80309.

* Corresponding author address: Daniel A. Rajewski, Iowa State University, 3132 Agronomy Ames, IA 50011. E-mail: drajewsk@iastate.edu

1 **Capsule summary:** CWEX demonstrates the importance of collecting field
2 measurements within a wind farm to facilitate basic understanding of the 3-way
3 interactions among wind energy, meteorology, and crop agriculture.
4

5 Abstract
6

7 Perturbations of mean and turbulent wind characteristics by large wind turbines modify
8 fluxes between the vegetated surface and the lower boundary layer. While simulations
9 have suggested that wind farms could significantly change surface fluxes of heat,
10 momentum, moisture, and CO₂ over hundreds of square kilometers, little observational
11 evidence exists to test these predictions. Quantifying the influences of the “turbine layer”
12 is necessary to quantify how surface fluxes are modified and to better forecast energy
13 production by a wind farm. Changes in fluxes are particularly important in regions of
14 intensely managed agriculture where crop growth and yield are highly dependent on
15 subtle changes in moisture, heat, and CO₂. Furthermore, speculations abound about the
16 possible mesoscale consequences of boundary-layer changes that are produced by wind
17 farms. To address the lack of observations to answer these questions, we developed the
18 Crop/Wind-energy EXperiment (CWEX) as a multi-agency, multi-university field
19 program in central Iowa. Throughout the summer of 2010, surface fluxes were
20 documented within a wind farm test site, and a two-week deployment of a vertically
21 pointing LIDAR quantified wind profiles. In 2011, we expanded measurements at the
22 site by deploying six flux stations and two wind-profiling LIDARs to document turbine
23 wakes. The results provide valuable insights into the exchanges over a surface that has
24 been modified by wind turbines and a base for a more comprehensive measurement
25 program planned for the summer in 2013.

1. Introduction

The United States Department of Energy (DOE) has outlined a scenario describing how wind power can be a major contributor to meet future U.S. renewable energy needs (DOE 2008). The “20% Wind Energy by 2030” report outlines steps for achieving 20% of the nation’s electrical energy from wind by 2030, a tenfold increase from the current level of 2% (AWEA 2010). Most of the richest land-based domestic resources of wind power in the United States are located in the central United States (North and South Dakota, Minnesota, Iowa, Illinois, Nebraska, Kansas, Oklahoma, Texas). Therefore, the DOE 20% by 2030 scenario will likely create additional interest in expanding the number of wind farms in this region. These states also produce most of the nation’s wheat and corn for food, livestock feed, or bio-fuel. Iowa alone accounts for 19% of the nation’s production of corn as well as 15% of soybean (USDA 2012). Much of this production is on the same land now being considered for wind farms.

While the co-location of wind farms with intensively managed agricultural production is possible, it leads to physical interactions between two otherwise separate economic systems. Crop selection and management determines surface drag and fluxes that influence hub-height wind speeds. By contrast, turbine-generated changes in mean wind, pressure, and turbulence may influence fluxes of heat, moisture, and CO₂ that are of vital importance to biophysical crop processes. Because multi-megawatt turbines and their access roads require less than half an acre of land, farmers often continue to graze livestock and farm crops right up to turbines’ bases (UCSUSA 2010). However, because the wakes of wind turbines are known to persist up to 15 rotor diameters (D) downwind of a turbine (Meyers and Meneveau 2012), differences in microclimate may extend well

beyond the wind turbines' small footprint on the landscape. As a result, some agronomists and producers have questioned whether or not the atmospheric impacts of wind turbines may also influence the biological productivity of the surrounding crops (personal discussion 2009). Therefore our goal for CWEX is to develop a basic understanding of how this land-use co-location changes both the energy and crop production systems that contribute to the nation's food and energy security needs. Originally, CWEX was launched to address the following four agronomic questions:

1. Do turbines create measureable changes in microclimate over crops?
2. If Q1 is true, are these changes large enough to produce measureable influences on plant growth?
3. If Q1 and Q2 are true, are these changes sufficient to have measureable impact on yield?
4. Do agricultural cropping and surface management practices have a measureable impact on wind energy production?

For this study we will report on the first of these questions and the other three will be topics of future CWEX experiments.

Two summer measurement campaigns were conducted to observe surface and elevated meteorological conditions in a wind farm co-located with agricultural fields. In the summer 2010 experiment, designated CWEX-10, the National Laboratory for Agriculture and the Environment (NLAE) deployed four flux stations in corn fields within a wind farm in central Iowa. The University of Colorado conducted upper-air observations for a portion of the summer. The second summer measurement period, CWEX-11, coincided with a 10-week Iowa State University summer program of the

1 National Science Foundation Research Experiences for Undergraduates (REU) in Wind
2 Energy Science, Engineering and Policy (WESEP). In support of the WESEP REU, the
3 Earth Observing Laboratory (EOL) of the National Center for Atmospheric Research
4 (NCAR) provided an educational deployment of instruments to the wind farm consisting
5 of four surface flux stations, and included operational support and data archives. Iowa
6 State University (ISU) provided two flux stations for CWEX-11. The National
7 Renewable Energy Laboratory and the University of Colorado provided two wind-
8 profiling LIDARs to observe wind and turbulence profiles during CWEX-11.

9 Numerous discussions with representatives from the agricultural, wind energy,
10 and boundary-layer meteorology communities about the summer field measurement
11 campaigns have affirmed that the extension of CWEX to a more comprehensive field
12 program offers a unique opportunity to create a deeper understanding of the range of
13 basic and applied science issues.

14 Section 2 describes the CWEX site, highlighting its use for current and future
15 field campaigns to address these critical questions. The experimental design and
16 instrumentation are described in Section 3. An analysis of surface flux differences is
17 presented in Section 4, and a case study of the differences in fluxes and in wind and
18 turbulence profiles is in Section 5. In Section 6 we demonstrate the potential influence of
19 turbines on daytime crop-canopy fluxes of heat and carbon dioxide. Lastly in Section 7,
20 we present an expanded list of science questions and prospects for future campaigns and
21 solicit engagement from the academic, national laboratory, and private sector segments of
22 the agronomic, wind-energy and boundary-layer/mesoscale meteorology communities.

2. Site Description

The CWEX experiments were conducted within a 200-turbine (1.5 MW rated power) wind farm in central Iowa. The wind farm features GE 1.5 MW sle model turbines (rated wind speed of 14 m s^{-1}) with hub-heights of 80 m and rotor diameters of 74 m for the southernmost 100 turbines and GE 1.5 MW xle model turbines (rated wind speed of 11.5 m s^{-1}) with rotor diameters of 77 m and 82.5 m for the northern 100 turbines. Additional turbine specifications are available from GE and in their 1.5 MW wind turbine brochure (2009). The land generally is flat with less than a 0.5-degree slope from southwest to northeast. Crops in the wind farm were a patchwork of mostly corn and soybeans, with some wetland and lower terrain at the southern edge of the wind farm. Measurements were taken at the southwest edge of the farm, as shown in Fig.1, to explore crop-turbine-boundary-layer interactions in the vicinity of the leading line of turbines, designated as the B-turbine line, for the predominant wind direction, (S to SSE) in mid to late summer. Climatological wind roses for the nearby Marshalltown airport document prevailing winds for the months of January (Fig. 2a) and July (Fig. 2b). Additional wind roses are available from the Iowa Environmental Mesonet: http://mesonet.agron.iastate.edu/sites/windrose.phtml?network=IA_ASOS. Within the study area is a second line of turbines, designated as the A-turbine line, 1.7 km to the north of the leading line, and a third line, designated as the C-turbine line, is located 1.8 km southeast of the turbine line of our CWEX-10/11 measurement site.

For both CWEX-10 and CWEX-11 measurements were collected above and within a corn canopy. At the start of each experiment (late June), the crop height was about 1.5 m, and by the second to third week of July the canopy reached its maximum

height near 2.8 m. Roughness length varied from 0.05 m to approximately 0.4 m for neutral stratification conditions, which closely follows the parameterization of $1/10^{\text{th}}$ the canopy height (Campbell and Norman 1998).

3. CWEX measurement design

To address our initial question, CWEX-10 was designed to examine differences in surface fluxes and mean variables at several locations in the vicinity of one line of turbines. Several offshore studies suggest that turbine wake interaction with the surface would be detected beyond 5-10 D downwind from the turbines (e.g. Barthelmie et al. 2010). Preliminary profile measurements of temperature and 2-m wind speed above a soybean canopy were taken at the wind farm around the A and B line of turbines in 2009. One mast was held stationary at a distance of 3-4 D upwind of the line of turbines and depending on the wind direction the other mast was moved every 20 minutes at intervals of 1 D downstream of the turbine line. Differences in surface mean wind speed, turbulence intensity, and thermal instability were observed at a few locations within 2-3 D behind the turbines, but impacts were diminished in the 5-7 D range and the results from these simple studies were the impetus for the larger experiments conducted in CWEX-10/11.

For CWEX-10, four surface flux stations, designated NLAE 1-4 in Fig. 1, were provided by the National Laboratory for Agriculture and the Environment. The upwind flux tower in CWEX-10 was placed about 4.5 D south of the B-turbine line to measure characteristics of the undisturbed flow of the prevailing southerly winds. A second flux

tower sampled a near-wake position about $2.5 D$ north of the B-turbine line. The third
 flux tower was located $17 D$ from the B-turbine line for observations at a ‘far-wake’
 location. A fourth flux tower was placed north of the A-turbine line about $35 D$
 downstream of the B-turbine line to capture the influence of wakes from two lines of
 turbines. The significant variability of turbine wakes observed in CWEX-10
 demonstrated the need for detailed measurements of surface flux differences at closer
 distances from the leading line of turbines. Therefore, in CWEX-11, more flux towers
 were deployed closer to the B-turbine line. The upwind reference tower (NCAR 1) was
 placed $2.0 D$ south of turbine B2. The northerly (downwind) flux towers (NCAR 2,
 NCAR 3, and NCAR 4) were placed at $3.5 D$, $9 D$, and $14 D$, respectively, north of
 turbine B2. Two additional flux towers, designated as ISU 1 and ISU 2, were placed
 north and south of the midpoint between turbines B2 and B3, at approximately $2.0 D$
 upwind and $3.5 D$ downwind.

From data collected by the Windcube LIDAR (version 1, manufactured by
 Leosphere and NRG Systems, Inc.) that was deployed for two weeks in CWEX-10, we
 learned that sufficient particulate loading within the boundary layer in this location
 enabled high quality wind and turbulence profiles to be collected as a complement to
 surface-based measurements. The LIDAR could “see” to 120 m above the surface over
 95% of the time (Aitken et al. 2012). As a result, two LIDARs, designated as WC 68 and
 WC 49, were deployed in CWEX-11 to observe wind and turbulence profiles at
 approximately $2.0 D$ south and $3.5 D$ north of turbine B3.

Flux stations in CWEX-10 and CWEX-11 had similar instrumentation (e.g. sonic
 and cup anemometers), but not all measurements were collected at identical heights or

1 with the same type of sensor. Table 1 provides lists of the key instrumentation used in
2 the two years of the study.

3 Data from the sonic anemometers, krypton hygrometers, and gas analyzers were
4 collected at 20 Hz, whereas other flux station sensors sampled every 1 Hz, and the wind
5 and turbulence profiles were collected every 0.5 Hz. CWEX-10 was conducted from 27
6 June to 7 September 2010. We report herein only measurements taken when the
7 turbines were operational. In CWEX-11, flux measurements and wind profiles were
8 archived for the period 29 June to 16 August 2011.

9 One lesson learned from CWEX-10/11 is the inherent variability of the cropland
10 within the wind farm, even in the rather featureless terrain of CWEX, due to variations in
11 soil type, drainage quality, and land management practices (tillage, row spacing, cultivar
12 type, planting date, and chemical applications). These factors influence crop growth and
13 therefore fluxes of heat, moisture, CO₂, and momentum within and above the crop
14 canopy. Direct comparison of CWEX-10 and CWEX-11 differences in the flux data also
15 are complicated by the contrasts in growing season weather. Conditions during CWEX-
16 10 were abnormally wet, whereas the summer of 2011 was much drier. No clear change
17 in crop roughness was observed from the two distinctly different growing seasons. The
18 following section provides the results of surface fluxes from CWEX-10, in which
19 similarities were observed to the data from CWEX-11.

20

1 4. Detection of turbine-induced surface flux differences

2 We used the wind direction from the near-wake flux tower (NLAE 2 in CWEX-
3 10 and NCAR 2 in CWEX-11) to distinguish between wake and non-wake periods
4 (periods when an individual wake from turbine B2 or B3 was most likely overhead of the
5 flux station). For hub height wind speeds below 15 m s^{-1} , Barthelmie et al. (2010)
6 observed that as wakes advect downwind, they tend to expand by five degrees within the
7 first 10 D downwind. The same procedure also was applied in CWEX-11 for determining
8 the turbine B3 wake for southerly flow and westerly flow non-wake periods for the
9 LIDAR data. The wind directions that represent the influence of wake for NLAE 2,
10 NCAR 2 and WC 49 are marked on the upwind wind roses for NLAE 1, NCAR 1, and
11 WC 68, respectively (Fig. 3a-c). The plots demonstrate the importance of measuring
12 wind speed and direction at multiple elevations near the turbines, especially under
13 thermally-stratified nighttime conditions when the turbines are operating within or
14 underneath a low-level jet environment that includes significant speed and directional
15 shear.

16 To investigate the flux differences attributable to the turbine B2 in 2010 we
17 considered the wind direction window 189° - 221° to give a wake over the NLAE stations,
18 for which we had a total of 420 15-min observations. These were compared to
19 observations with westerly flow (248° - 282°) that gave no wake over the NLAE stations,
20 for which we had 413 observations. We also present a SSE flow condition (151° - 189°)
21 for which NLAE 2 was between the wakes of turbine B2 and B3. For this wind direction
22 window we had 574 observations. The differences in conditions between flux towers
23 north and south of the B-turbine line were compared for daytime and nighttime

1 conditions. We used the common scaling of thermal stability (z/L_0) at the reference flux
 2 tower, where z is the height of the sonic anemometer (6.5 m in CWEX-10 and 4.5 m in
 3 CWEX-11). The Obukhov length at the reference flux tower, L_0 , is defined following
 4 Stull (1988):

$$5 \quad L_0 = \frac{-\overline{\theta}_v u_*^3}{k g (\overline{w' \theta'_v})_s}$$

6 and k is von Karman's constant (0.4), u_* is the friction velocity, $\overline{\theta}_v$ is the surface virtual
 7 potential temperature, and $(\overline{w' \theta'_v})_s$ is the surface moist sensible heat flux defined over a 15-
 8 minute averaging period.

9 Differences between the reference station (NLAE 1) and the flux towers (NLAE
 10 2, NLAE 3, NLAE 4) north of the B turbine line demonstrate the influence of turbines at
 11 6.5 m in the turbulence and sensible heat flux and at 9 m for the mean wind speed and air
 12 temperature (Fig. 4). We calculate a normalized wind speed difference, $\left(\frac{u-u_0}{u_0}\right)$ and TKE
 13 difference $\left(\frac{TKE-TKE_0}{TKE_0}\right)$ with respect to the undisturbed upwind reference speed, u_0 , and
 14 turbulence kinetic energy, TKE_0 , at the same height according to the analysis methods for
 15 simulating shelterbelt wind break flow in Wang and Takle (1995). Tables 2 to 5 quantify
 16 the mean and spread of the normalized wind speed, TKE, air temperature, and the
 17 sensible heat flux respectively, for each stability class and flux station north and south of
 18 the B-line of turbines for flow from the west (non-wake), SW (B2 wake), and the SSE
 19 (flow between the wakes of turbines B2 and B3). We classify each set of differences
 20 into three categories of the reference stability: unstable ($z/L_0 < -0.05$), neutral (-

1 $0.05 \leq z/L_0 \leq 0.05$), and stable ($z/L_0 > 0.05$). Notable values are marked with a double
 2 asterisk in Tables 2-5.

3 The non-wake westerly flow in Fig. 4a,d shows considerable scatter in the wind
 4 speed and TKE for all stability conditions but the overall mean difference is near zero at
 5 the NLAE 2 and NLAE 3 flux towers. For this (westerly) flow direction the data from
 6 NLAE 4 should be considered inconclusive since they may in some cases be influenced
 7 by the four turbines to the west of the A-line (shown in the wind farm layout in Fig. 1).

8 For a narrow window of southwesterly flow the wake of turbine B2 is overhead
 9 our line of flux stations. Wind speeds are reduced (by 10-40%) in neutral to slightly
 10 unstable conditions at NLAE 2 and NLAE 4 but this effect is negligible at NLAE 3 (Fig.
 11 4b). The difference in wind speed between NLAE 2 and NLAE 1 reveals a slow-down
 12 in the near-wake of the turbine, whereas at NLAE 3 there is a slight speed recovery,
 13 presumably because higher speed air from above has begun to replenish the near-turbine
 14 deficit. At NLAE 4 there is an aggregated influence from both the B-turbine line and the
 15 A-turbine line. The surface-level wind speed reductions we report are in agreement with
 16 daytime velocity deficits at tall tower masts for an isolated turbine or groups of turbines
 17 in on-shore coastal studies (e.g. Höglström et al 1988, Magnusson and Smedman 1994).
 18 For stable-flow, the number of observations is low, but a relatively high percentage of
 19 these observations show a speed-up at all flux towers north of the B line of turbines.
 20 TKE measurements (Fig. 4e) for the nighttime B2 wake condition show substantial
 21 enhancement at all stations downwind of B2, but we note high variability in the
 22 normalized TKE (Table 3). For the daytime flow, by contrast, the characteristically large

TKE at the reference station is enhanced only modestly ($<20\%$) by the turbine as measured at downwind stations.

For SSE winds the NLAE 2 flux station is between the wakes of turbines B2 and B3. As shown in Fig. 4c, the northern two flux towers detect higher nighttime over-speeding (e.g., speeds downwind of the turbine being larger than the upwind reference speed) than at NLAE 2, which demonstrates the expanding influence of multiple wakes beyond $10 D$ from the B-line of turbines. Under stably-stratified nighttime conditions, this localized jet is not rapidly dissipated by turbulent exchange, whereas more turbulent neutral conditions suppress the tendency for wind speed enhancement. We revisit nighttime over-speeding in Section 5. There are clear effects of enhanced TKE (4-5 times TKE_0) at NLAE 4 from the combined influence of the A and B lines of turbines. NLAE 3 has higher TKE (2.5 times TKE_0) than the near wake location at NLAE 2, which we attribute to the aforementioned expansion of multiple wakes several tens of D downstream from the B line. Turbulence at NLAE 2 is slightly enhanced, likely due to the over-speeding at this location. Although Fig. 4f demonstrates substantial differences in the normalized TKE for stable flow at all three stations downwind of the B-turbine line we detect high variability among the individual cases. TKE is enhanced at the northern flux stations when the upstream turbulence is very low.

We observed a slight cooling ($< 0.75\text{ }^{\circ}\text{C}$) at 9 m during the daytime for the two northernmost stations in the southwest B2 wake and south-southeast B2 and B3 gap conditions (Fig. 4h and 4i) but temperature contrasts between NLAE 2 and NLAE 1 are generally less than $0.5\text{ }^{\circ}\text{C}$ as are all differences in the daytime westerly case (Fig 4g). For nighttime periods the scatter of temperature differences is high for west wind

conditions, and lack of data prevents analysis of temperature impacts for the B2 wake case. However, for south-southeast winds we anticipate wakes from the B2 and B3 to spread out and reach the surface somewhere near NLAE 3. At the northernmost flux station (NLAE 4), we see a compounding influence of both B and A turbines to produce several individual periods with a significant warming of 1.0-1.5 °C. Although the variability is high (Table 4), we observe nighttime warming at NLAE 4 similar to that reported at the downwind edge of the San Gorgonio wind farm and statistically analyzed in comparison to airport data by Baidya Roy and Traiteur (2010).

In our report of sensible heat flux differences we caution that the fluxes are derived from the sonic temperature without making a correction for the humidity in the air. Moisture correction was not possible at NLAE 3 and NLAE 4 since these stations did not measure H₂O and CO₂ and therefore could not record fluxes of these constituents. The “uncorrected” sensible heat flux shows significant scatter of daytime differences for all three directional categories (Fig. 4 j-l). For stable conditions we would expect turbine-generated turbulence to be enhancing downward heat flux if the turbine wake is intersecting with the surface. Overall, the data do not show a systematic and significant influence of the turbines on the surface sensible heat flux, although in Fig. 4l we notice a few observations with slightly larger heating at NLAE 4 (up to 40 W m⁻²) for south-south-easterly flow. Future CWEX experiments will sample surface heat fluxes deeper in the wind farm, where multiple wakes prevail, for comparison with those near the windward lines of turbines reported herein where single wakes and gaps between wakes are more prevalent.

The CWEX-11 results showed similar results for the southerly B2 wake observations (wind directions from 165°-195°) and exhibited the same daytime speed reductions, nighttime accelerations, and increases in TKE. These data also revealed decrease (increase) in daytime (nighttime) temperature and a modest increase in downward heat transport (25 W m^{-2}) especially at the northernmost flux station (NCAR 4). However, the nighttime heat flux at NCAR 4 (CWEX-11) was weaker than what was observed at the NLAE 4 (CWEX-10), which we attribute to the influence of wakes from multiple lines of turbines.

5. Turbine wake influences on wind and turbulence profiles: *a case study, night of 16-17 July 2011*

A case study is presented to show the coupling between wake aloft and surface processes. The overnight period of 16-17 July 2011 featured southerly flow within the wind farm during a convection-free and cloud-free period. The dew-point depression was less than 2°C, but airport Automated Surface Observing System (ASOS) stations near the wind farm recorded visibilities of two to three standard nautical miles or greater (NCAR 2011). A synoptic-scale backing pattern was revealed in the flux station and LIDAR observations. The undisturbed wind profile (Fig. 5a) indicated winds steadily increasing with height, with a maximum between 12 and 14 m s^{-1} at 220 m above the surface, and this persisted throughout the night. The wake characteristics in Fig. 5c can be quantified by subtracting the downwind observations (Fig. 5b) from the upwind observations. The

1 momentum deficit of the wake occurs in the layer of the turbine rotor disk (40 m to 120
 2 m), with some expansion in the vertical to 140 m. The largest wake deficits of $\sim 6 \text{ m s}^{-1}$
 3 occurred at 100 m (which is above the 80-m hub height) and represent a speed decrease
 4 of 40%. The lowest level of Windcube observations, 40 m above the surface, suggests
 5 some slight acceleration below the wake, but these wind speed differences were small,
 6 being less than 1 m s^{-1} .

7 The standard deviations of velocities measured by the LIDAR are used to estimate
 8 TKE using the following relationship:

$$9 \quad TKE_{lidar} = \frac{1}{2} (\sigma_u^2 + \sigma_v^2 + \sigma_w^2)$$

10 where σ_u , σ_v , and σ_w , represent the standard deviations of the zonal, meridional, and
 11 vertical wind components, respectively. Some reports have indicated disagreement
 12 between LIDAR turbulence metrics and those from *in situ* instruments (Sathe et al.
 13 2011); however, the purpose herein is comparison of two LIDAR measurements, not a
 14 strict calculation of TKE at one location *per se*. Upwind, downwind, and difference
 15 time-height cross-sections of LIDAR estimates of TKE (Fig. 6) corroborate previous
 16 studies (Högström et al. 1988, among others) showing TKE increases in the wake. We
 17 observed that TKE enhancement was confined to the turbine rotor disk layer during the
 18 night, with some lofting occurring after sunrise as convective eddies lifted from the
 19 surface. In the mid-morning through early afternoon there is slight expansion of turbine
 20 turbulence to about 20 m above the rotor layer. We expect a sharp decrease of turbulence
 21 above the rotor layer during the night as the temperature stratification prevents vertical
 22 mixing of these larger eddies and sustains the ambient “upwind” turbulence above the
 23 turbines.

Wake effects were also revealed in the 15-min averages of the surface fluxes. As found in CWEX-10, the region below the wake experiences significant over-speeding (0.5 to 1.0 m s^{-1}) not only at the near-wake location (NCAR 2), but also at the far-wake tower (NCAR 4). Data from the ISU flux towers located between turbine wakes exhibit less over-speeding than for the flux stations directly downwind of turbine B2 (Fig. 7a). We present differences in the data from two ISU towers and the reference NCAR tower, but caution that the differences in measurement height (8 m vs. 10 m) are responsible for the higher speeds for the NCAR sites. Wake effects on TKE show a similar pattern (Fig. 7b): the NCAR flux stations directly north of turbine B2 exhibit TKE enhancements of as much as $0.30 \text{ m}^2 \text{ s}^{-2}$, whereas there is negligible difference in turbulence between the two stations in the gap region (ISU 2 - ISU 1) when wind directions are between 170° - 180° . However, for the wind direction near 160° , the turbulence at ISU 2 increases as the edge of the B3 wake has shifted over the flux tower, and conversely, the turbulence is reduced at the NCAR stations north of turbine B2 as the edge of the wake has moved to the left of the line of the NCAR flux stations.

We observe slightly larger difference in 10-m temperature (0.3 K) between the gap stations at 10 m (Fig. 7c), whereas the NCAR stations do not report any significant warming downstream of turbine B2. However for the 4.5 m sonic temperature (Figure not shown) there is roughly a 0.5 K difference between NCAR 4 and NCAR 1 with lower contrasts (0.25 - 0.4 K) between the upwind flux tower and the near-wake (NCAR 2) or intermediate location (NCAR 3). The 4.5 m temperature difference in the gap region is the smallest of any plotted ($\pm 0.1 \text{ K}$), being about 0.25 K higher downwind only when a wind direction from 160° from 0330 to 0500 LST positions the edge of the wake over the

1 ISU 2 flux station. Measurements of sensible heat flux in far-wake locations (NCAR 3-
 2 4) show a larger downward heat flux by $15\text{-}20\text{ Wm}^{-2}$ as compared to the enhancement at
 3 the near-wake position (NCAR 2). For periods with flow slightly oblique to the tower
 4 line (near 160°) the heat flux difference between NCAR 2 and NCAR 1 is reduced,
 5 whereas the ISU 2-ISU 1 difference indicates more downward heat transport within the
 6 B3 wake above the ISU station.

7 We conclude that, for this southerly wind case, the turbine wakes from B2 and B3
 8 are confined to an approximately five degree expansion and do not impact the ‘gap’
 9 stations (ISU 1 and ISU 2). Further, the over speeding and enhancement of TKE at
 10 NCAR 4 are near the magnitudes observed at NCAR 2, but the effect is less noticeable at
 11 NCAR 3. Perhaps this is an indication that the turbine wake reaches the surface beyond
 12 10 D downstream of an individual turbine for this nighttime case.

13 Interpretation of observed winds and TKE near the turbine line calls for a more
 14 refined conceptual model of the pressure field, which we adopt from our previous
 15 modeling and measurements around agricultural shelterbelts (Wang et al. 2001). The
 16 turbines present a barrier to the flow, which creates a stationary (assuming a constant
 17 wind speed and wind direction) perturbation pressure field at the surface, with high
 18 pressure upwind and low pressure downwind. The largest increases in speed and
 19 turbulence behind the turbines occur at NCAR 2, which is consistent with a perturbation-
 20 pressure-driven speed-up immediately behind the turbine. The over speeding and the
 21 reduction of TKE at the ISU 2 flux tower between turbines B2 and B3 suggests that the
 22 differences in wind speed are also forced by the perturbation pressure fields around each

turbine. Our results suggest a need for future exploration of the perturbation pressure and flow effects around individual turbines and around multiple lines of wind turbines.

6. Turbine influences on fluxes of heat and carbon dioxide

Exchanges of CO₂, moisture, and heat between atmosphere and crops have important agricultural, as well as microclimate and mesoscale-flow consequences. Figure 8 provides a contrast between the 30-min average fluxes of sensible and latent heat and the carbon dioxide for the daytime southwesterly flow case of 18 July 2011 and the daytime frontal case of 2 Aug 2011. The Webb-Pearman Leuning correction (Webb et al. 1980) was applied to the latent heat and CO₂ fluxes. Skies were generally clear in both cases except for a period of cloudiness from 1250-1345 LST on Aug 2 (delineated by the vertical dashed lines in (b, d, and f)). The sensible heat flux difference between NCAR 3 and NCAR 1 is slightly larger on Aug 2 compared to Jul 18 but neither showed large change over the course of the day. Downwind-upwind latent heat flux differences for the two days (c) and (d) are similar in the morning hours. After the cloudiness period on Aug 2 the NCAR 3 – NCAR 1 difference in the latent heat flux suggests a sign reversal, which is in contrast to a positive mean value for the afternoon of Jul 18. The vertical flux differences of carbon dioxide (e) and (f) are similar in the morning with higher downward flux downwind of the turbines. In the afternoon (after the period of cloudiness on Aug 2) the fluxes are essentially identical on Aug 2, whereas for the July 18 the morning pattern is preserved. These data show that changes in relative magnitude

of the latent heat flux and CO₂ flux take place at the same time as the change in wind direction. These are consistent with (but perhaps not proof of) turbines creating an increase in upward latent heat flux and downward CO₂ flux over the crop during the daytime.

7. Remaining science questions and future campaigns

CWEX-10/11 provided evidence of changes in flow structures around single turbines or single lines of turbines and evidence suggesting turbines modify fluxes of importance to crops (e.g., heat and CO₂). Our analysis of these data, together with our previous experience from modeling and measurements of the aerodynamics of agricultural shelterbelts (Wang et al. 2001) lead us to propose three mechanisms that influence surface micrometeorological conditions in the near lee of turbines: (1) wind turbine wakes overhead that have not reached the surface but modify the wind profile, scales of turbulence, and the vertical mixing between the surface and the overlying boundary layer, (2) wind turbine wakes that are intersecting the surface allowing wake turbulence to modify the surface microclimate, and (3) static pressure fields (high pressure upwind and low pressure downwind) around each turbine and line of turbines which generate perturbations in surface flow (e.g., localized over speeding) and fluxes within a few D of the turbine line. Additional analyses of CWEX-10/11 data and future CWEX experiments to map out the pressure fields will further explore these proposed mechanisms.

The experiments thus far do not provide measurements of plant growth and yield influences of turbines (addressing questions 2-4 in the Introduction). CWEX-10/11

demonstrated that turbines very likely have positive (e.g., enhanced daytime CO₂ flux down into the crop canopy) and negative (e.g., higher nighttime temperature which enhances respiration) effects over short time periods. However, variability within and between fields due to cultivar, soil texture and moisture content, and management techniques create large uncertainties for attributing season-long biophysical changes, much less yield, to turbines alone. A caveat to this statement is that we have not sampled the center of the wind farm where aggregate effects of multiple rows of turbines may be more pronounced. Enlarging the study domain would allow this and other agronomic questions to be addressed. For instance staging an intensive observation period during the corn pollination period (mid-July to early August) offers a unique opportunity to study the transport and viability of pollen throughout the atmospheric boundary layer. In addition to conducting biophysical studies of pollen, this experiment could use pollen as a passive tracer for studying mesoscale influences of the wind farm (see the discussion below).

There is additional motivation for studying the impact of the wind farm as a whole as a basic science question, in addition to informing future siting and operation of wind farms. For instance better understanding is needed on how the mean and turbulent flow fields of the turbine layer interact with the overlying boundary layer and how this changes from day to night when (at least in summer in the central US) a strong low-level jet becomes established with peak winds within a few hundred meters of the surface. Additional unknowns relate to mesoscale influences on the flow fields around and over the wind farm, which has area of about 150 km². What are the impacts on low-level ($z < 100$ m) convergence patterns around the wind farm and vertical velocities above or

1 downwind of the wind farm at 200 m, 500 m, and top of the boundary layer? Do they
2 correspond with the impacts suggested by wind farm parameterizations in mesoscale
3 models (Baidya Roy et al. 2004; Barrie and Kirk-Davidoff 2010; Baidya Roy 2011; Fitch
4 et al. 2012)? Are these changes in convergence patterns sufficient to change patterns of
5 boundary-layer clouds (e.g. via gravity wave formation in wind farms described by Smith
6 2009)? Are the resulting magnitudes of changes sufficient to reorganize convectively
7 driven systems leading to precipitation or to change non-convective forcing of
8 precipitation (e.g., isentropic lift, CSI, and mesoscale banding, as discussed in Fiedler and
9 Bukovsky 2011)? Effects of mesoscale terrain, such as the Loess Hills feature along the
10 Iowa side of the Missouri River, which can generate a very shallow short-wave train
11 close to the surface, could potentially interact with wind farm dynamics. The activity of
12 this shallow short-wave train may lead to the fluctuation of surface winds across the wind
13 farm under stable night-time flow.

14 Finally, numerical modeling using Large Eddy Simulation (LES) and other high-
15 resolution models is needed to explore how a wind farm interacts with ambient
16 meteorological conditions to create local winds, transports, and stresses on wind turbine
17 components. A deeper understanding of these interactions is needed for improved
18 forecasts of wind power output by individual turbines within the wind farm and the forces
19 and stresses (possibly leading to blade and gearbox damage) likely to accrue from spatial
20 and temporal changes in turbulence patterns. Databases of field measurements from
21 operating wind farms are needed to validate a variety of wind-tunnel and numerical
22 simulation models (Chamorro and Porté-Agel 2009; Calaf et al. 2010; Churchfield et al.

1 2010; Cal et al. 2011; Lu and Porté-Agel 2011; Porté-Agel et al. 2011; Churchfield et al.
2 2012).

3 Current plans call for erection of two 120-m towers in the vicinity of the wind
4 farm for additional vertical measurements in future CWEX experiments. A community
5 call is planned to invite participation of other measurement teams for an expanded field
6 program in the summer of 2013 that will address the many science and application
7 questions we have raised. NCAR data from CWEX-11 are available from the CWEX-11
8 data archive website of the Earth Observing Laboratory of NCAR:
9 <http://www.eol.ucar.edu/deployment/educational-deployments/CWEX11>. Other data
10 from CWEX-10 and CWEX-11 will be become available in the near future from the Iowa
11 Environmental Mesonet (<http://mesonet.agron.iastate.edu/index.phtml>). Researchers
12 interested in joining future CWEX experiments should contact co-author E. S. Takle.

13 *Acknowledgments.*

14 This work was supported in part by the National Renewable Energy Laboratory under
15 Professor Lundquist's Joint Appointment. NREL is a national laboratory of the U.S.
16 Department of Energy, Office of Energy Efficiency and Renewable Energy, operated by
17 the Alliance for Sustainable Energy, LLC. Partial funding for CWEX-10 was provided
18 by the Ames Laboratory (DOE) and the Center for Global and Regional Environmental
19 Research at the University of Iowa. Surface flux stations for CWEX-11 were provided by
20 NCAR Earth Observing Laboratory under an instrumentation deployment, and
21 undergraduate student participation was supplemented by funding from an NSF REU
22 program under grant 1063048. Data analysis was supported in part by the National
23 Science Foundation under the State of Iowa EPSCoR Grant 1101284.

1 **References**

- 2 Aitken, M. L., M. E. Rhodes, and J. K. Lundquist, 2012. Performance of a wind-profiling
3 lidar in the region of wind turbine rotor disks. *J. Atmos. and Oceanic Technol.*, **29**, 347-
4 355. doi: <http://dx.doi.org/10.1175/JTECH-D-11-00033.1>.
- 5
- 6 American Wind Energy Association, cited 2011: U.S. wind industry year-end 2010
7 market report. [Available online at
8 http://www.awea.org/leanabout/publications/upload/4Q10_market_outlook_public.pdf.]
9
- 10 Baidya Roy, S., 2011: Simulating impacts of wind farms on local hydrometeorology. *J.*
11 *Wind Eng. Ind. Aerodyn.*, **99**, 491–498, doi: 10.1016/j.jweia.2010.12.013.
- 12
- 13 Baidya Roy, S., and J. Traiteur, 2010: Impact of wind farms on surface temperatures.
14 *Proc. Natl. Acad. Sci.*, **107**, 17899–17904, doi: 10.1073/pnas.1000493107.
- 15
- 16 Baidya Roy, S., S. W. Pacala, and R. L. Walko, 2004: Can large wind farms affect local
17 meteorology? *J. Geophys. Res.*, **109**, D19 101, doi: 10.1029/2004JD004763.
- 18
- 19 Barthelmie, R. J., and Coauthors, 2010: Quantifying the Impact of Wind Turbine Wakes
20 on Power Output at Offshore Wind Farms. *J. Atmos. Oceanic Technol.*, **27**, 1302–1317.
21 doi: <http://dx.doi.org/10.1175/2010JTECHA1398.1>.

1 Barrie, D. B. and D. B. Kirk-Davidoff, 2010: Weather response to a large wind turbine
2 array. *Atmos. Chem. Phys.*, **10**, 769–775, doi: 10.5194/acp-10-769-2010.

3
4 Cal, R. B., J. Lebron, L. Castillo, H. S. Kang, and C. Meneveau, 2011: Experimental
5 study of the horizontally averaged flow structure in a model wind-turbine array boundary
6 layer. *J. Renewable Sustainable Energy*, **2**, 013 106, doi: 10.1063/1.3289735.

7
8 Calaf, M., C. Meneveau, and J. Meyers, 2010: Large eddy simulation study of fully
9 developed wind-turbine array boundary layers. *Phys. Fluids*, **22**, 015 110, doi:
10 10.1063/1.3291077.

11
12 Campbell, G.S., and J.M. Norman, 1998: *An Introduction to Environmental Biophysics*.
13 2nd ed. Springer –Verlag, 286 pp.

14
15 Chamorro, L. and F. Porté-Agel, 2009: A wind-tunnel investigation of wind-turbine
16 wakes: Boundary-layer turbulence effects. *Bound.-Layer Meteor.*, **132**, 129–149,
17 doi:10.1007/s10546-009-9380-8.

18
19 Churchfield, M.J. et al., 2010. Wind Energy-Related Atmospheric Boundary Layer
20 Large-Eddy Simulation Using OpenFOAM: Preprint. In *19th Symposium on Boundary*
21 *Layers and Turbulence*, Keystone, CO, Amer. Meteor. Soc., 1-26. [Available online at
22 http://ams.confex.com/ams/19Ag19BLT9Urban/techprogram/paper_172636.htm.]
23

Churchfield, M. J., S. Lee, J. Michalakes, and P. J. Moriarty, 2012: A Numerical Study of the Effects of Atmospheric and Wake Turbulence on Wind Turbine Dynamics. Submitted and accepted to *Journal of Turbulence*.

Fiedler, B. H. and M. S. Bukovsky, 2011: The effect of a giant wind farm on precipitation in a regional climate model. *Environ. Res. Lett.* 6:045101. doi: 10.1088/1748-9326/6/4/045101.

Fitch, Anna C., Joseph B. Olson, Julie K. Lundquist, Jimmy Dudhia, Alok K. Gupta, John Michalakes, Idar Barstad, 2012: Local and Mesoscale Impacts of Wind Farms as Parameterized in a Mesoscale NWP Model. *Mon. Wea. Rev.*, **140**, 3017–3038. doi: <http://dx.doi.org/10.1175/MWR-D-11-00352.1>

General Electric Energy, cited 2009: 1.5 MW Wind Turbine. [Available online at www.ge-energy.com/wind.]

Högström, U., D. N. Asimakopoulos, H. Kambezidis, C.G. Helmis, and A. Smedman, 1988: A field study of the wake behind a 2 MW wind turbine. *Atmos. Environ.*, **22**, 803–820. [http://dx.doi.org/10.1016/0004-6981\(88\)90020-0](http://dx.doi.org/10.1016/0004-6981(88)90020-0).

Lu, H. and F. Porté-Agel, 2011: Large-eddy simulation of a very large wind farm in a stable atmospheric boundary layer. *Phys. Fluids*, **23**, 065 101, doi:10.1063/1.3589857.

- 1 Magnusson, M., and A. S. Smedman, 1994: Influence of atmospheric stability on wind
2 turbine wakes. *Wind Eng.*, **18**, 139–151.
- 3
- 4 Meyers, J., and C. Meneveau, 2012: Optimal turbine spacing in fully developed wind-
5 farm boundary layers, *Wind Energ.*, **15**, 305-317. doi:10.1002/we.469.
- 6
- 7 National Center for Atmospheric Research, cited 2011: National Center for Atmospheric
8 Research-Mesoscale and Microscale Division Image Archive Meteorological case study
9 selection kit. [Available online at <http://locust.mmm.ucar.edu>.]
- 10
- 11 Porté-Agel, F., Y.-T. Wu, H. Lu, and R. J. Conzemius, 2011: Large-eddy simulation of
12 atmospheric boundary layer flow through wind turbines and wind farms. *J. Wind Eng.*
13 *Ind. Aerodyn.*, **99**, 154–168, doi: <http://dx.doi.org/10.1016/j.jweia.2011.01.011>.
- 14
- 15 Sathe, A., J. Mann, J. Gottschall, and M. S. Courtney, 2011: Can wind lidars measure
16 turbulence? *J. Atmos. Oceanic Technol.*, **28**, 853–868.
17 doi: <http://dx.doi.org/10.1175/JTECH-D-10-05004.1>.
- 18
- 19 Smith, R.B., 2009: Gravity wave effects on wind farm efficiency. *Wind. Energ.*, **13**, 449-
20 458. doi: 10.1002/we.366.
- 21
- 22 Stull, R., 1988: *An Introduction to Boundary Layer Meteorology*. Kluwer Academic
23 Publishers, 666 pp.

Union of Concerned Scientists, cited 2011: Farming the wind: wind power and agriculture. [Available online at http://www.ucsusa.org/clean_energy/technology_and_impacts/impacts/farming-the-wind-wind-power.html.]

U.S. Department of Agriculture, National Agricultural Statistics Service, cited 2012: Crop production 2011 summary January 2012, 95 pp; USDA Report No. 1057 -7823. [Available online at <http://www.usda.gov/nass/PUBS/TODAYRPT/cropan12.pdf>.]

U.S. DOE Office of Energy Efficiency and Renewable Energy, 2008: 20% Wind Energy by 2030: Increasing Wind Energy's Contribution to U.S. Electricity Supply, 248 pp.; NREL Report No. TP-500-41869; DOE/GO-102008-2567. [Available online at <http://www.nrel.gov/docs/fy08osti/41869.pdf>.]

Wang, H., and E. S. Takle, 1995: A numerical simulation of boundary-layer flows near shelterbelts. *Bound.-Layer. Meteor.*, **75**, 141-173.

Wang, H., E. S. Takle, and J. Shen, 2001: Shelterbelts and windbreaks: Mathematical modeling and computer simulation of turbulent flows. *Ann. Rev. Fluid Mech.*, **33**, 549-586.

- 1 Webb, E.K., G.I. Pearman, and R. Leuning, 1980. Correction of flux measurements for
- 2 density effects due to heat and water vapor transfer. *Quart. J. Roy. Meteorol. Soc.*, **106**,
- 3 85-100.

Article IN PRESS

1 **List of Figures**

2 FIG. 1. Overlay of the wind farm boundaries with an expanded view of the measurement
3 locations for CWEX-10 and CWEX-11.

4
5 FIG. 2. Climatological 10-m wind roses of the Marshalltown airport for the months of (a)
6 January and (b) July.

7
8 FIG. 3. Wind roses for (a) CWEX-10 6.5-m winds at the reference flux tower (NLAE 1),
9 (b) CWEX-11 10-m winds at the reference flux tower (NCAR 1), and (c) CWEX-11 80-
10 m winds from the upwind wind cube (WC 68). Dashed lines denote wind directions for
11 turbine wakes on downwind stations.

12
13 FIG. 4. CWEX-10 differences (downwind – upwind) of normalized wind speed and
14 normalized TKE, 9-m air temperature, and uncorrected sensible heat flux as functions of
15 upwind flux tower thermal stability (z/L_0): for the westerly no-wake case (a),(d),(g),and
16 (j); for the SW B2 turbine wake case (b),(e),(h),and (k); and for the SSE case between the
17 wakes of turbine B2 and B3 (c),(f),(i),and (l).

18
19 FIG. 5. Contours of wind speed from (a) WC 68, (b) WC 49, and (c) calculated
20 difference in wind speed attributed to the wind turbine wake effect. Overlay with a solid
21 black line is for the top of the rotor height and the dashed black line indicates the hub
22 height.

23

1 FIG. 6. Time-height cross sections of (a) upwind TKE profile, (b) downwind TKE
 2 profile, and (c) difference between (a) and (b). Overlay with a solid black line is for the
 3 top of the rotor height and the dashed black line indicates the hub height.

4
 5 FIG. 7. Differences during the night of 16-17 July 2011 for (a) wind speed (b) TKE, (c)
 6 air temperature, and (d) sensible heat flux. Note that at the ISU tower wind speed and
 7 temperature are collected at the 8-m level while the NCAR tower wind speed and
 8 temperature are observed at 10 m.

9
 10 FIG. 8. Comparison of differences in 30-min averaged fluxes of sensible heat (a-b), latent
 11 heat (c-d), and CO_2 (e-f) between NCAR 3 and NCAR 1 for a southerly wind case on 18
 12 July 2011 and for a transition from southerly to northwesterly direction on 2 Aug 2011.
 13 NCAR 3 10-m wind direction vectors are overlaid for each image. Dashed lines in (b),
 14 (d), and (f) denote the period of cloudiness during the transition of winds from southerly
 15 to northwesterly on the early afternoon of 2 Aug 2011.

16

1 TABLE 1. Instrumentation type, sensor height, and location for flux stations operating
 2 during CWEX-10 and CWEX-11. More detailed specifications of each sensor in the
 3 following footnotes #1-8.

<i>Sensor type</i>	<i>Height above ground (m) CWEX-10</i>	<i>Location for CWEX-10</i>	<i>Height above ground (m) CWEX -11</i>	<i>Location for CWEX-11</i>
Sonic anemometer ^{1,*}	6.5	NLAE 1-4	4.5	NCAR 1-4 ISU 1-2
Net radiometer ²	6.5	NLAE 1-2	4.5	ISU 1-2
Gas analyzer ^{3,**}	6.5	NLAE 1-2	4.5	NCAR 1,3 ISU 1
Cup/Prop anemometer ⁴	9.0	NLAE 1-4	10 8, 3	NCAR 1-4 ISU 1-2
Temp-RH probe ⁵	5.3, 9.0	NLAE 1-4	10, 2 8, 3, 1	NCAR 1-4 ISU 1-2
Tipping bucket ⁶	5.2	NLAE 1-4	3.3	ISU 1-2
Air pressure ⁷	6.5	NLAE 1-2	2 4.5	NCAR 1-4 ISU 1
Leaf wetness ^{8,***,****}			2 1.7	NCAR 1 ISU 1-2

4

5

- ¹ CSAT3, [Campbell Scientific Inc., Logan UT] - ^{*} possible 0.6° C warm bias at NLAE 1
- ² CNR1 and CNR4 [Kipp and Zonen, Delft, The Netherlands] for ISU 1-2; Q7.1 REBS [REBS, Inc., Bellevue, WA] for NLAE 1-2
- ³ LI-7500, [Li-Cor Biosciences, Lincoln, NE] for NLAE 1-2, NCAR 1,3; EC-150 [Campbell Scientific, Inc., Logan UT] for ISU 1 - ^{**} H₂O flux measured with Krypton hygrometer at NCAR 2,4
- ⁴ 03101 Wind Sentry [Campbell Scientific Inc., Logan UT] for NLAE 1-4 and ISU 1-2; 05103 Wind Monitor [R.M. Young, Traverse City, MI] for NCAR 1-4
- ⁵ HMP40/45C [Campbell Scientific Inc., Logan UT] for NLAE 1-4 and ISU 1-2; HMP50 [Campbell Scientific Inc., Logan UT] for ISU 1-2; NCAR SHT-75 thermo-hygrometer with aspiration systems for NCAR 1-4
- ⁶ TE-525 [Texas Electronics, Inc., Dallas, TX]
- ⁷ LI-7500 for NLAE 1-2; EC-150 for ISU 1; PTB 220 [Vaisala, Helsinki, Finland] for NCAR 1-4
- ⁸ Leaf wetness sensor [Decagon Devices, Inc., Pullman, WA] - ^{***} measured on the NCAR 1 tower, ^{****} measured in the canopy

1 TABLE 2. CWEX-10 means and standard deviations (in parentheses) of the differences
2 (downwind – upwind) in normalized wind speed for upwind flux tower thermal stability
3 (z/L_0) categories: unstable, neutral, and stable for the westerly no-wake case; for the SW
4 B2 turbine wake case; and for the SSE gap case between the wakes of turbine B2 and B3.
5 Notable differences are indicated with double asterisks.
6

$\frac{\Delta U}{U_0}$		(NLAE 2-NLAE 1)	(NLAE 3-NLAE 1)	(NLAE 4-NLAE 1)
No wake (West)	unstable ($z/L_0 < -0.05$)	0.00 (0.24)	0.07 (0.18)	0.06 (0.28)
	neutral ($-0.05 < z/L_0 < 0.05$)	0.03 (0.21)	0.06 (0.14)	0.02 (0.17)
	stable ($z/L_0 > 0.05$)	0.02 (0.30)	0.10 (0.19)	0.16 (0.28)
B2 wake (SW)	unstable ($z/L_0 < -0.05$)	-0.10 (0.11)**	-0.01 (0.16)	-0.05 (0.32)
	neutral ($-0.05 < z/L_0 < 0.05$)	-0.12 (0.08)**	-0.03 (0.09)	-0.13 (0.12)**
	stable ($z/L_0 > 0.05$)	0.21 (0.56)	0.24 (0.34)	0.37 (0.84)
B2_B3 (SSE gap)	unstable ($z/L_0 < -0.05$)	-0.01 (0.16)	0.01 (0.21)	-0.04 (0.28)
	neutral ($-0.05 < z/L_0 < 0.05$)	-0.07 (0.06)**	0.01 (0.09)	-0.10 (0.12)**
	stable ($z/L_0 > 0.05$)	0.16 (0.28)	0.31 (0.23)**	0.22 (0.25)**

1 TABLE 3. CWEX-10 means and standard deviations (in parentheses) of differences
2 (downwind – upwind) in normalized TKE for upwind flux tower thermal stability (z/L_0)
3 categories: unstable, neutral, and stable for the westerly no-wake case; for the SW B2
4 turbine wake case; and for the SSE gap case between the wakes of turbine B2 and B3.
5 Notable differences are indicated with double asterisks.
6

$\frac{\Delta TKE}{TKE_0}$		(NLAE 2-NLAE 1)	(NLAE 3-NLAE 1)	(NLAE 4-NLAE 1)
No wake (West)	unstable ($z/L_0 < -0.05$)	0.05 (0.40)	0.26 (0.65)	0.21 (0.75)
	neutral ($-0.05 < z/L_0 < 0.05$)	0.07 (0.23)	0.25 (0.34)	0.18 (0.42)
	stable ($z/L_0 > 0.05$)	0.30 (1.08)	0.39 (0.66)	1.22 (1.98)
B2 wake (SW)	unstable ($z/L_0 < -0.05$)	0.12 (0.27)	-0.01 (0.79)	0.11 (0.51)
	neutral ($-0.05 < z/L_0 < 0.05$)	0.12 (0.20)	0.06 (0.21)	0.03 (0.27)
	stable ($z/L_0 > 0.05$)	2.68 (4.07)	1.89 (1.66) **	2.42 (2.37) **
B2_B3 (SSE gap)	unstable ($z/L_0 < -0.05$)	0.13 (0.26)	-0.16 (1.03)	0.18 (0.62)
	neutral ($-0.05 < z/L_0 < 0.05$)	0.09 (0.15)	0.06 (0.21)	0.05 (0.25)
	stable ($z/L_0 > 0.05$)	1.07 (1.46)	1.34 (1.26) **	1.61 (1.69) **

TABLE 4. CWEX-10 means and standard deviations (in parentheses) of the differences (downwind – upwind) of 9-m air temperature for upwind flux tower thermal stability (z/L_0) categories: unstable, neutral, and stable for the westerly no-wake case; for the SW B2 turbine wake case; and for the SSE gap case between the wakes of turbine B2 and B3. Notable differences are indicated with double asterisks.

ΔT ($^{\circ}C$)		(NLAE 2-NLAE 1)	(NLAE 3-NLAE 1)	(NLAE 4-NLAE 1)
No wake (West)	unstable ($z/L_0 < -0.05$)	-0.11 (0.73)	-0.14 (0.24)	-0.20 (0.26)
	neutral ($-0.05 < z/L_0 < 0.05$)	0.00 (0.49)	-0.05 (0.14)	-0.41 (2.04)
	stable ($z/L_0 > 0.05$)	-0.02 (0.69)	0.01 (0.32)	-0.08 (0.42)
B2 wake (SW)	unstable ($z/L_0 < -0.05$)	0.06 (0.14)	-0.19 (0.19)**	-0.11 (0.22)
	neutral ($-0.05 < z/L_0 < 0.05$)	-0.15 (1.29)	-0.13 (0.12)**	-0.08 (0.17)
	stable ($z/L_0 > 0.05$)	-0.04 (1.42)	0.05 (0.24)	-0.02 (0.32)
B2_B3 (SSE gap)	unstable ($z/L_0 < -0.05$)	-0.01 (0.14)	-0.14 (0.21)	-0.06 (0.27)
	neutral ($-0.05 < z/L_0 < 0.05$)	0.04 (0.08)	-0.08 (0.12)	0.00 (0.19)
	stable ($z/L_0 > 0.05$)	0.10 (0.24)	0.32 (0.25)**	0.43 (0.43)**

TABLE 5. CWEX-10 means and standard deviations (in parentheses) of the differences (downwind – upwind) uncorrected sensible heat flux for upwind flux tower thermal stability (z/L_0) categories: unstable, neutral, and stable for the westerly no-wake case; for the SW B2 turbine wake case; and for the SSE gap case between the wakes of turbine B2 and B3. Notable differences are indicated with double asterisks.

$\Delta H \text{ (W m}^{-2}\text{)}$		(NLAE 2-NLAE 1)	(NLAE 3-NLAE 1)	(NLAE 4-NLAE 1)
No wake (West)	unstable ($z/L_0 < -0.05$)	0.13 (15.13)	-12.31 (43.68)	11.37 (25.90)
	neutral ($-0.05 < z/L_0 < 0.05$)	5.40 (11.94)	- 2.98 (18.94)	13.03 (23.64)
	stable ($z/L_0 > 0.05$)	- 0.34 (7.76)	- 0.17 (6.18)	- 5.93 (9.60)
B2 wake (SW)	unstable ($z/L_0 < -0.05$)	0.23 (17.94)	- 0.89 (31.19)	14.74 (39.41)
	neutral ($-0.05 < z/L_0 < 0.05$)	- 0.08 (12.34)	6.99 (19.39)	10.98 (24.16)
	stable ($z/L_0 > 0.05$)	- 6.62 (17.04)	0.28 (23.58)	- 1.08 (14.96)
B2_B3 (SSE gap)	unstable ($z/L_0 < -0.05$)	- 9.07 (19.16)	-18.28 (36.25)	18.30 (37.58)
	neutral ($-0.05 < z/L_0 < 0.05$)	- 3.02 (11.38)	- 0.71 (19.18)	10.55 (27.10)
	stable ($z/L_0 > 0.05$)	- 6.06 (9.14)	- 6.24 (14.04)	-11.31 (12.94)

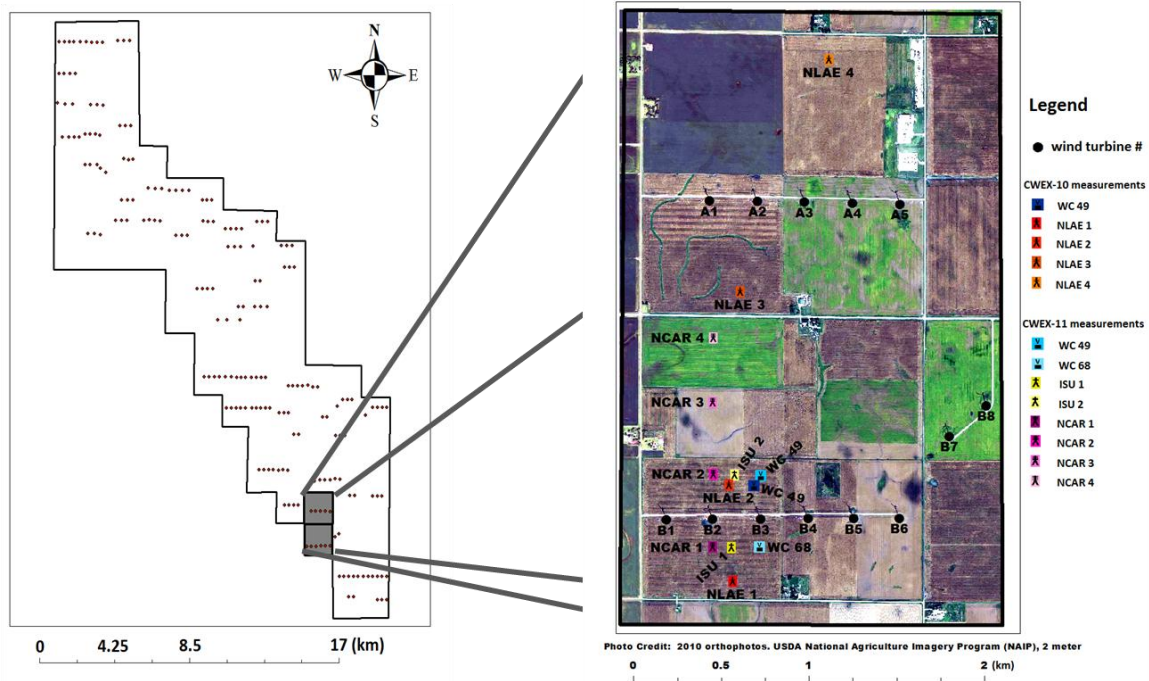


FIG. 1. Overlay of the wind farm boundaries with an expanded view of the measurement locations for CWEX-10 and CWEX-11.

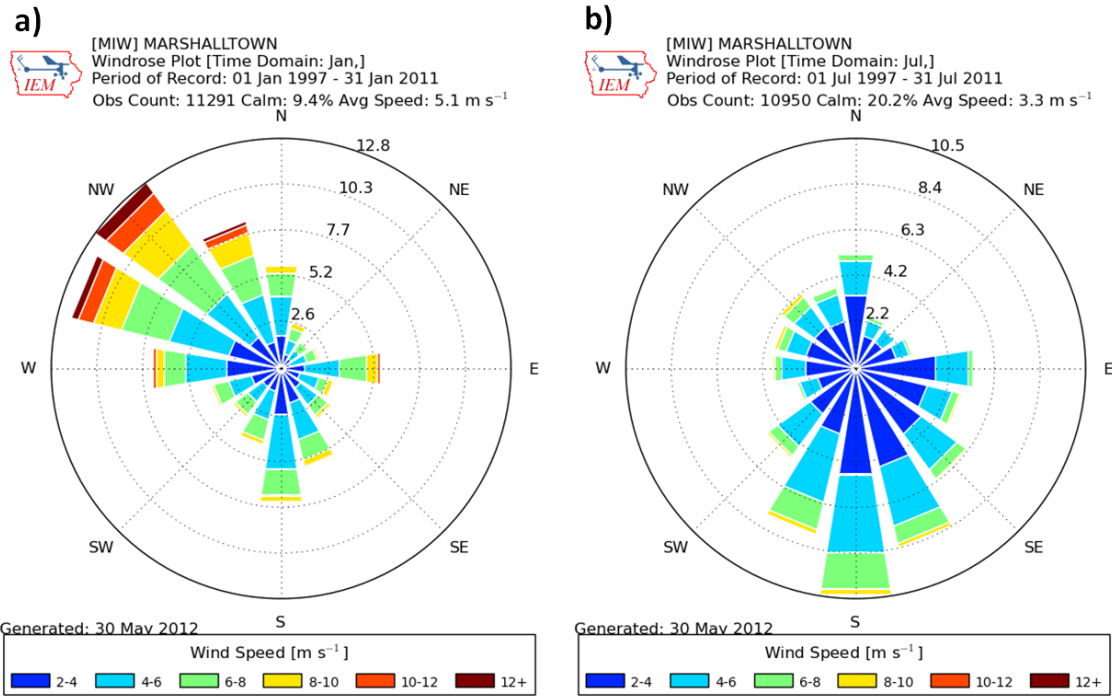
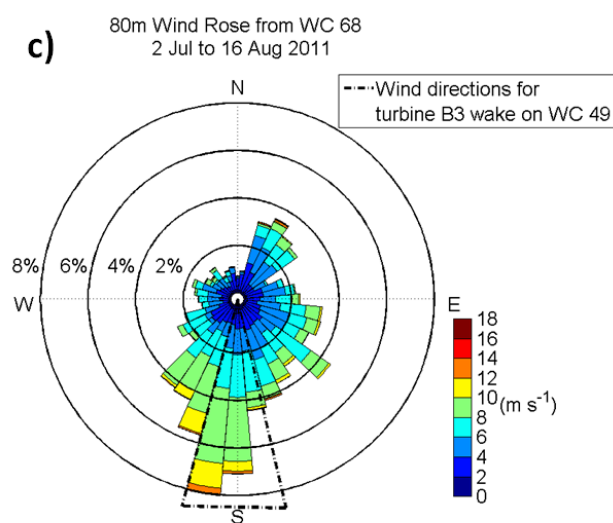
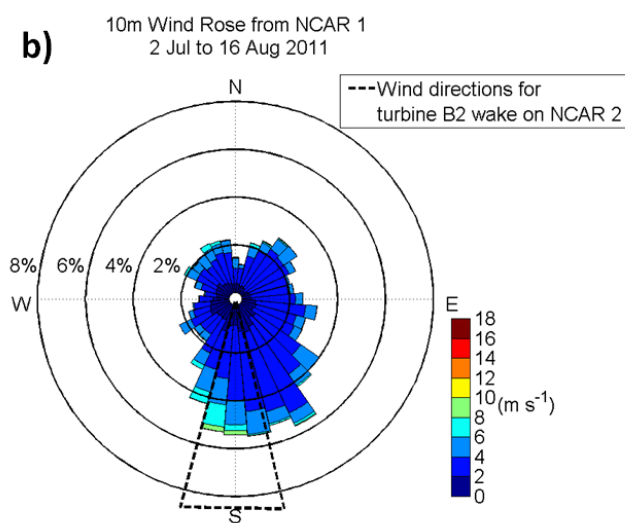
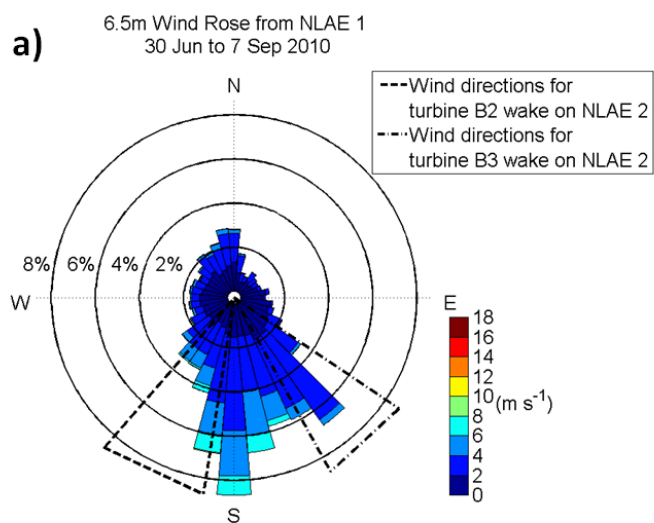


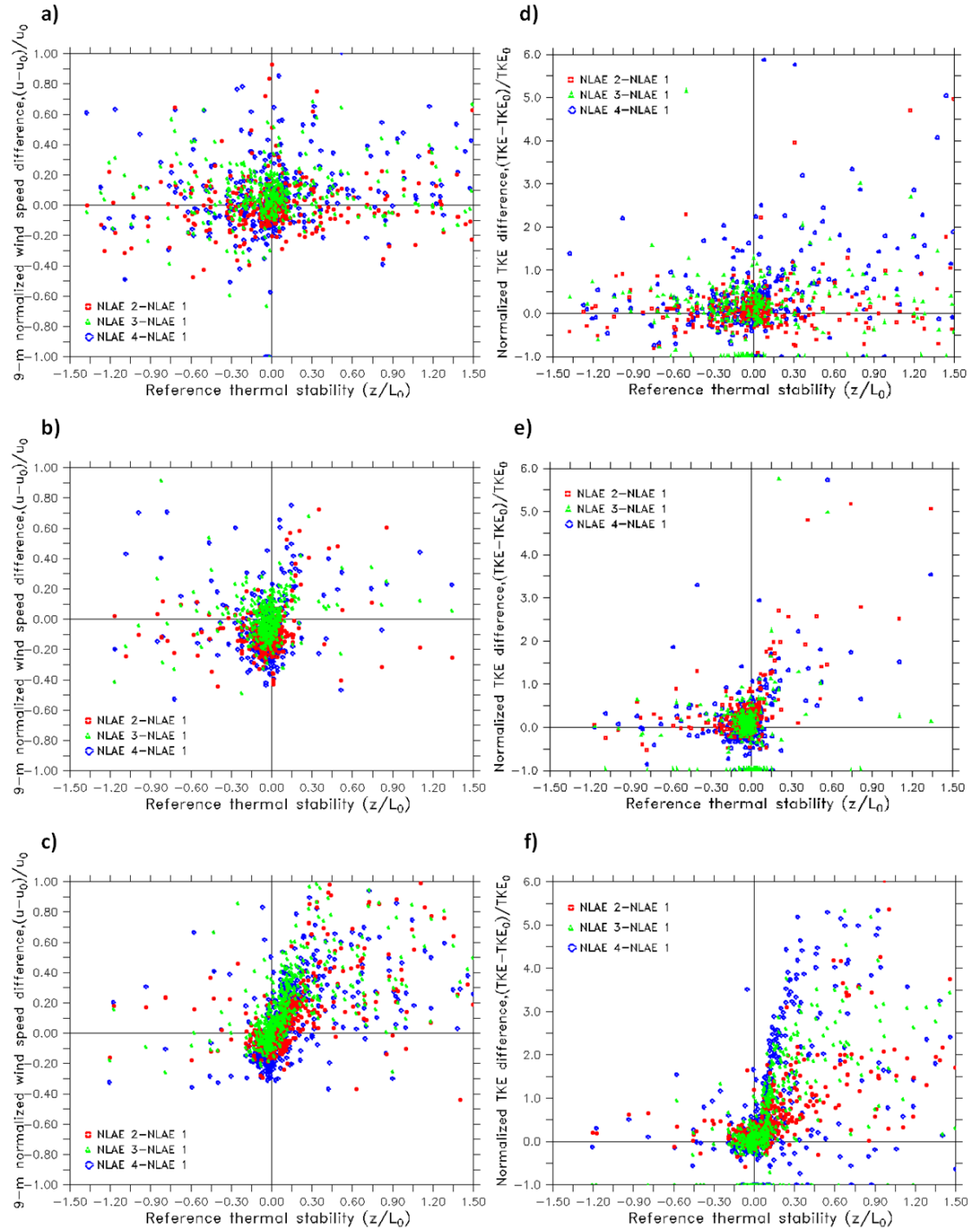
FIG. 2. Climatological 10-m wind roses of the Marshalltown airport for the months of (a) January and (b) July.

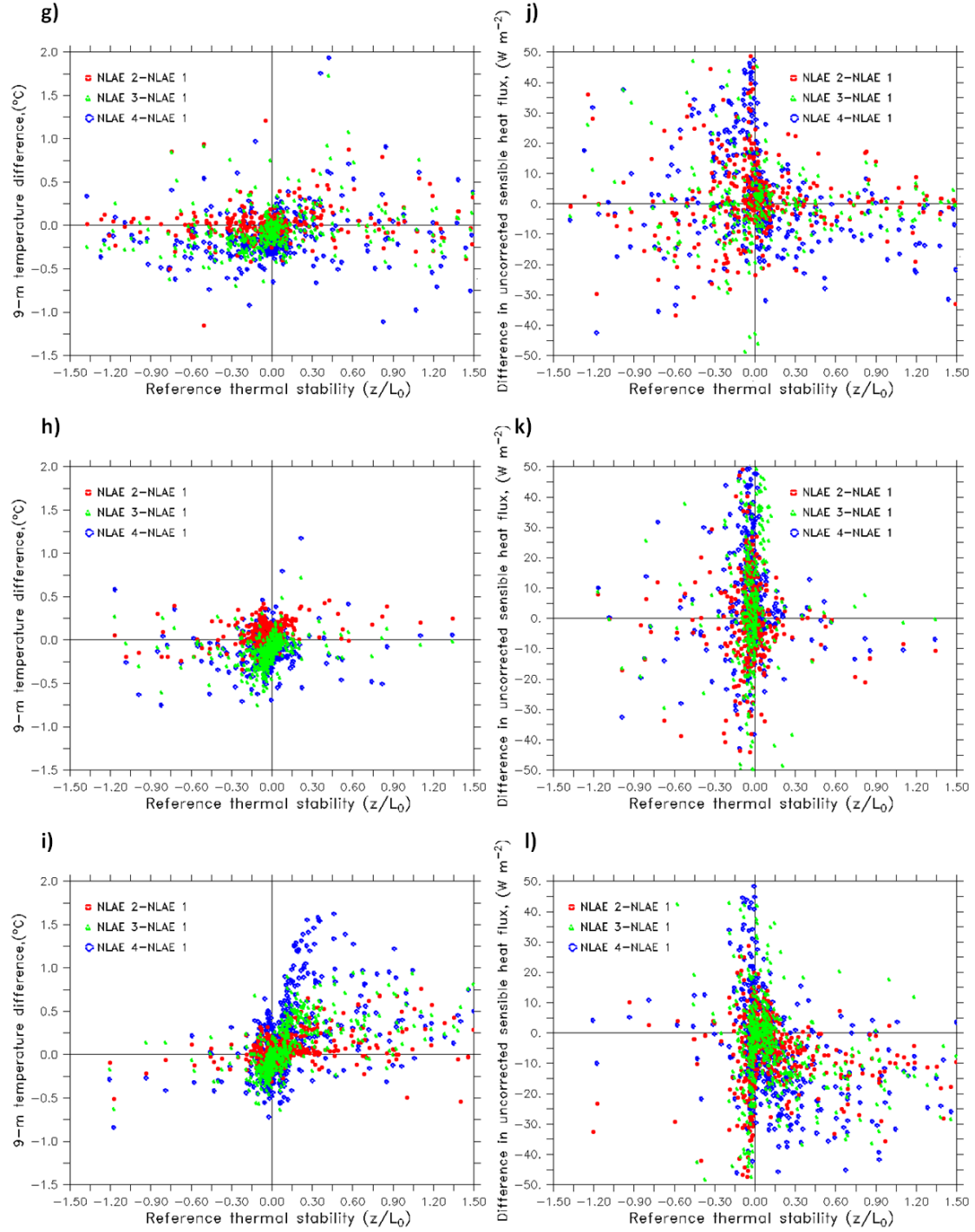


1 FIG. 3. Wind roses for (a) CWEX-10 6.5-m winds at the reference flux tower (NLAE 1),
2 (b) CWEX-11 10-m winds at the reference flux tower (NCAR 1), and (c) CWEX-11 80-
3 m winds from the upwind wind cube (WC 68). Dashed lines denote wind directions for
4 turbine wakes on downwind stations.

5

Article IN PRESS





1

2 FIG. 4. CWEX-10 differences (downwind – upwind) of normalized wind speed and
 3 normalized TKE, 9-m air temperature, and uncorrected sensible heat flux as functions of
 4 upwind flux tower thermal stability (z/L_0): for the westerly no-wake case (a),(d),(g),and

1 (j); for the SW B2 turbine wake case (b),(e),(h),and (k); and for the SSE case between the
2 wakes of turbine B2 and B3 (c),(f),(i),and (l).

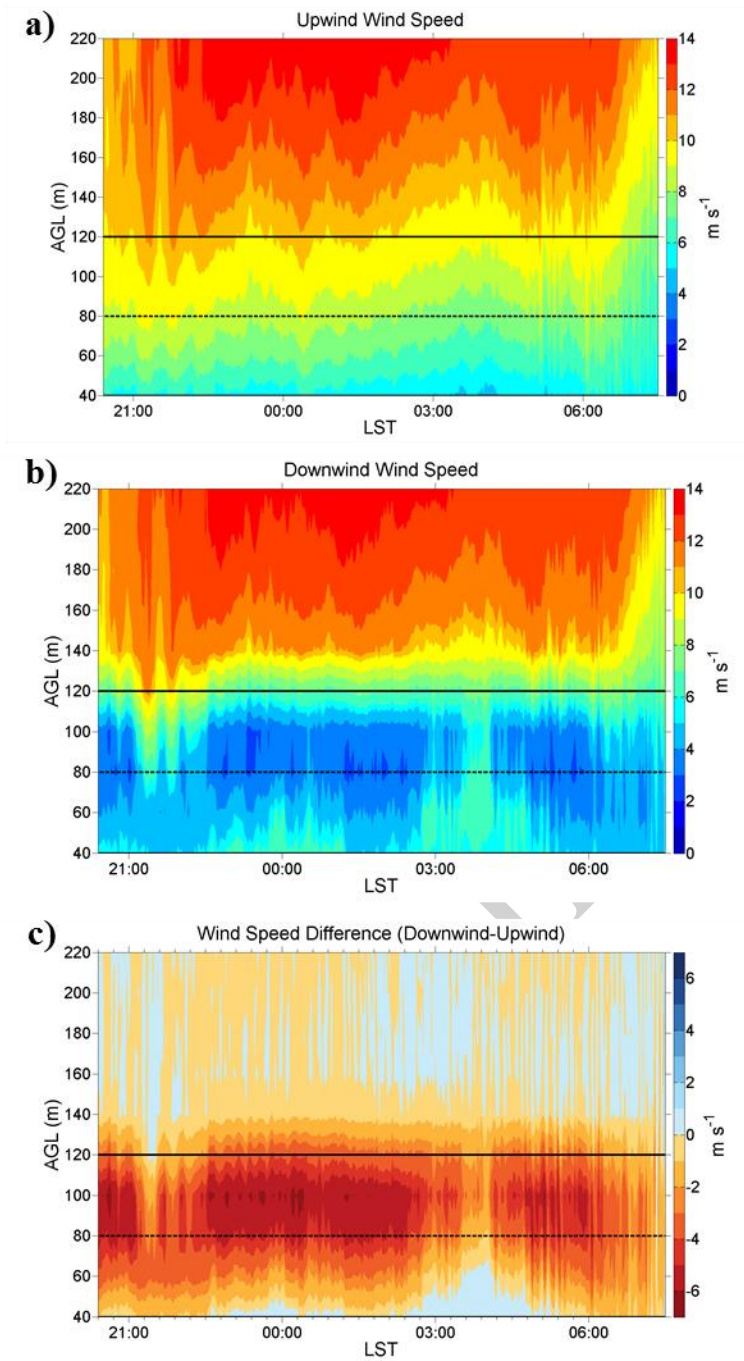
3

4

5

6

Article IN PRESS



1

2 FIG. 5. Contours of wind speed from (a) WC 68, (b) WC 49, and (c) calculated difference
 3 in wind speed attributed to the wind turbine wake effect. Overlay with a solid black line
 4 is for the top of the rotor height and the dashed black line indicates the hub height.

5

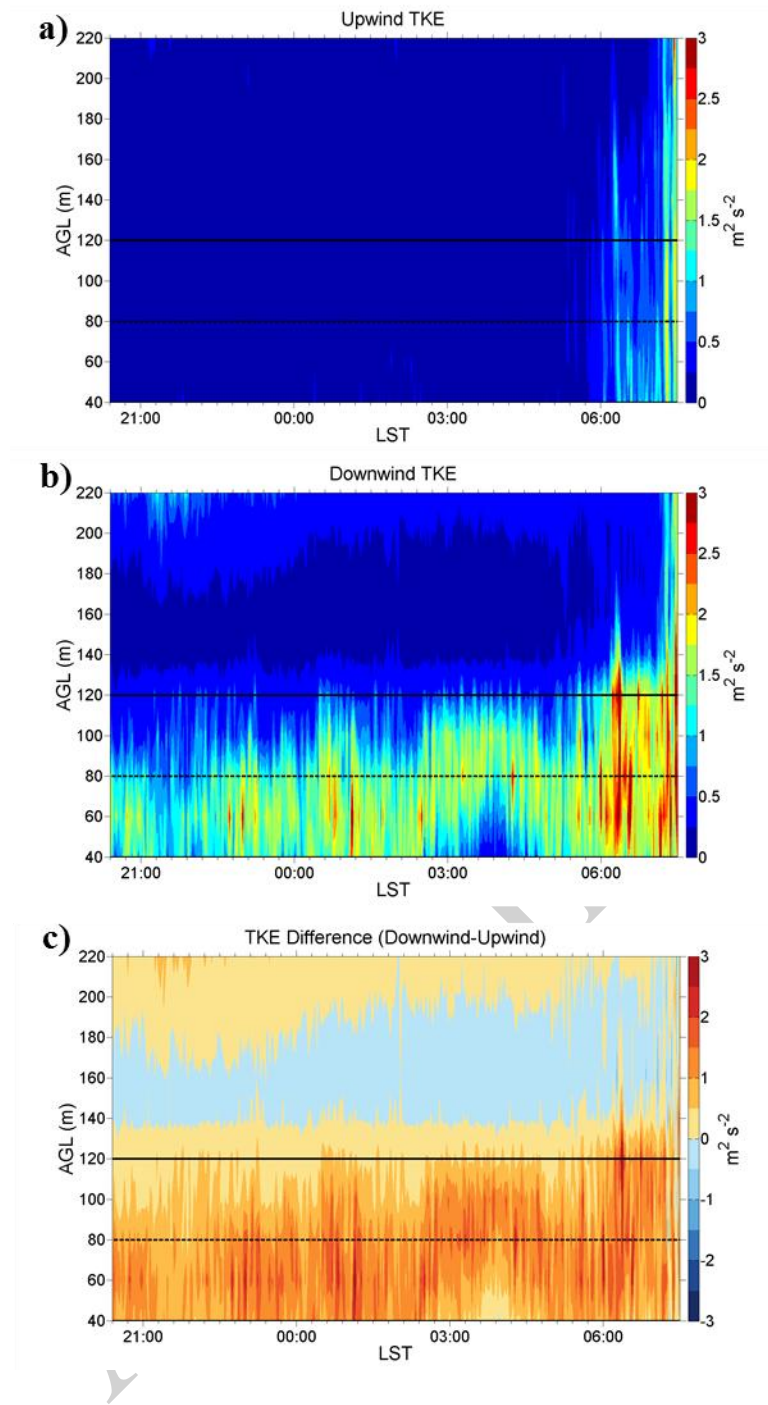


FIG.6. Time-height cross sections of (a) upwind TKE profile, (b) downwind TKE profile, and (c) difference between (a) and (b). Overlay with a solid line is for the top of the rotor height and the dashed line indicates the hub height.

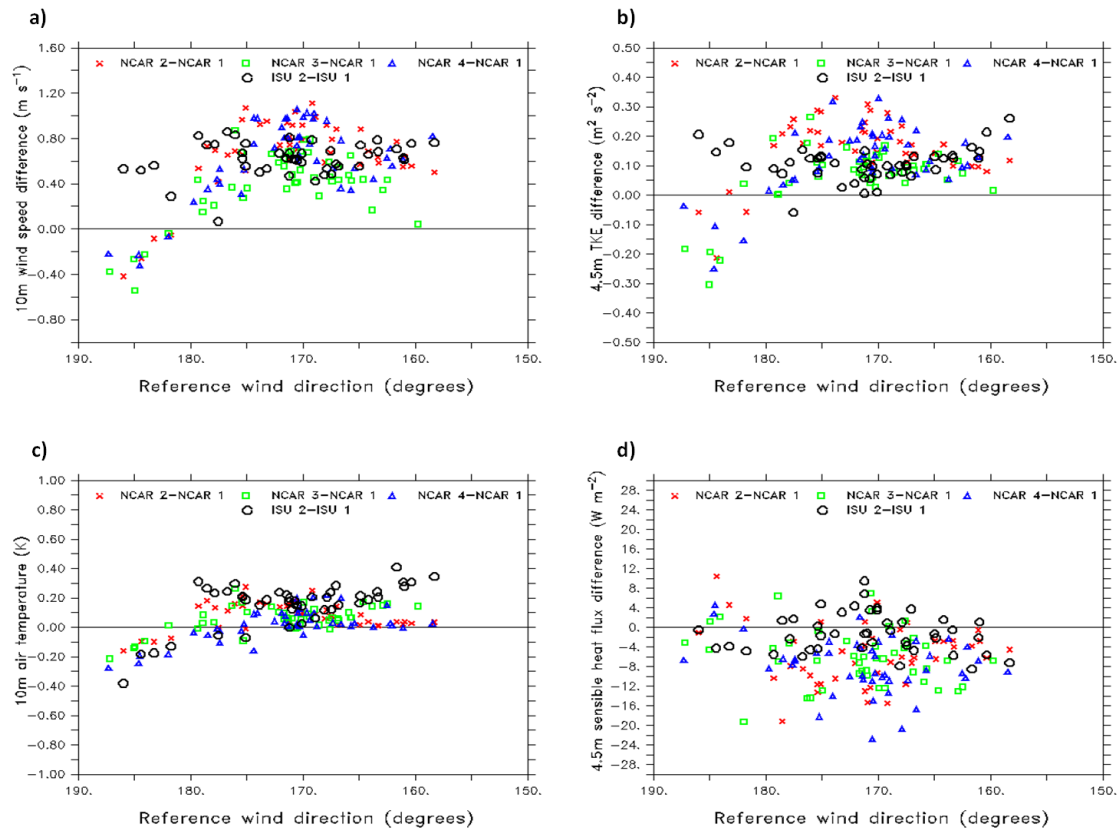
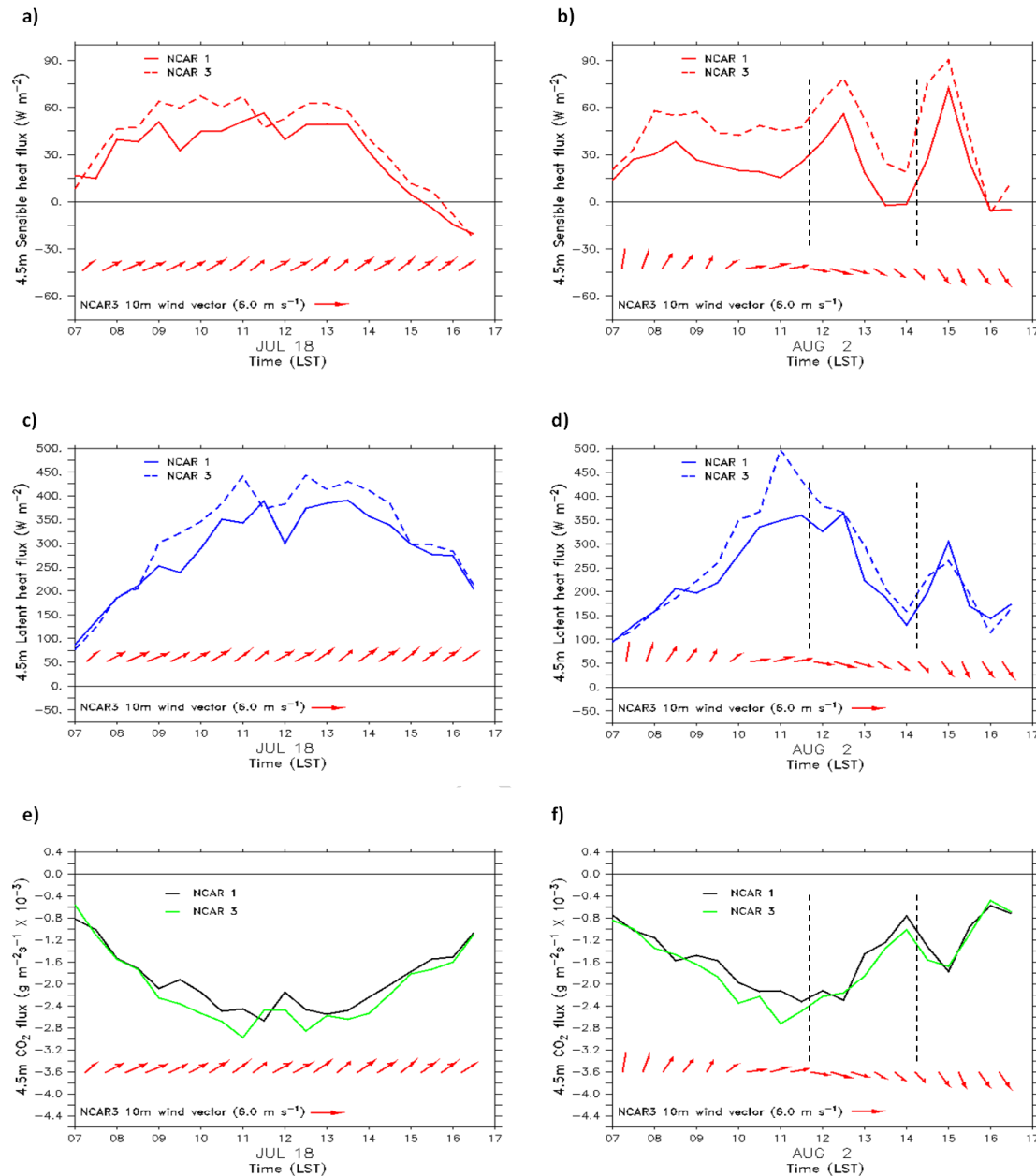


FIG. 7. Differences during the night of 16-17 July 2011 for (a) wind speed (b) TKE, (c) air temperature, and (d) sensible heat flux. Note that at the ISU tower wind speed and temperature are collected at the 8-m level while the NCAR tower wind speed and temperature are observed at 10 m.



1
2 FIG. 8. Comparison of differences in 30-min averaged fluxes of sensible heat (a-b), latent
3 heat (c-d), and CO_2 (e-f) between NCAR 3 and NCAR 1 for a southerly wind case on 18
4 July 2011 and for a transition from southerly to northwesterly direction on 2 Aug 2011.
5 NCAR 3 10-m wind direction vectors are overlaid for each image. Dashed lines in (b),

1 (d), and (f) denote the period of cloudiness during the transition of winds from southerly
2 to northwesterly on the early afternoon of 2 Aug 2011.

3

4

Article IN PRESS